Active Site Models for Galactose Oxidase. Electronic Effect of the Thioether Group in the Novel Organic Cofactor

Shinobu Itoh,* Shigehisa Takayama, Ryuichi Arakawa, Akihiro Furuta, Mitsuo Komatsu, Akito Ishida,† Setsuo Takamuku,† and Shunichi Fukuzumi*

Department of Applied Chemistry, Faculty of Engineering, Osaka University, 2-1 Yamada-oka, Suita, Osaka 565, Japan

Received September 18, 1996[⊗]

The electronic effect of the thioether linkage between Tyr 272 and Cys 228 (the novel organic cofactor) of galactose oxidase has been examined by using model compounds, 2-(methylthio)-*p*-cresol (**1H**), 2-(methylthio)-4,6-dimethylphenol (**2H**), and 2-(methylthio)-4-methyl-6-[[bis[2-(2-pyridyl)ethyl]amino]methyl]phenol (**3H**), the physicochemical properties of which are compared to those of 2-[[bis[2-(2-pyridyl)ethyl]amino]methyl]-4-methylphenol (**4H**) and *p*-cresol (**5H**). ^{1}H NMR and electrochemical studies indicate that the methylthio group has essentially an electron-donating nature. On the other hand, the lower pK_a values of **1H** and **2H** as compared to that of **5H** suggest that the methylthio group also has a 2pπ−3dπ electron conjugative effect, stabilizing the negative charge on the phenolate oxygen. Furthermore, the electron-sharing conjugative effect of the substituent in the radical state has been clearly demonstrated by ESR studies and semiempirical molecular orbital calculations. Dimer copper(II) complexes $[Cu^{II}_2(\mathbf{3}^-)_2](PF_6)_2$ (**7**) and $[Cu^{II}_2(\mathbf{4}^-)_2](PF_6)_2$ (**8**) were prepared, and the crystal structures were determined by the X-ray diffraction method. Electrochemical analyses of the monomeric species $[Cu^{II}(\mathbf{3}^-)(py)](PF_6)$ (**9**) and $[Cu^{II}(\mathbf{4}^-)(py)](PF_6)$ (**10**) generated *in situ* by adding an external ligand such as pyridine (py) reveal that the methylthio substituent in the copper complex shows electronic effects similar to those of the free ligand stabilizing the phenoxyl radical state of the cofactor moiety in the Cu(II) complex.

Introduction

Galactose oxidase (EC 1.1.3.9) is a copper enzyme that catalyzes the oxidation of D-galactose and primary alcohols to the corresponding aldehydes coupled to the reduction of O_2 to H_2O_2 (eq 1).[1] This enzyme is unusual among metalloenzymes,

$$RCH_2OH + O_2 \rightarrow RCHO + H_2O_2 \qquad (1)$$

since it catalyzes the two-electron redox reaction at a mononuclear metal ion center. In this context, it has been proposed that, in addition to the copper ion, there is a second organic cofactor acting as another one-electron redox center in the enzyme active site.[2−5] In 1991, a research group in Leeds, U.K., successfully determined the crystal structure of the enzyme at 1.7 Å resolution to demonstrate that there is a second organic cofactor posttranslationally derived from Tyr 272 and Cys 228 as illustrated in Scheme 1.[6] This built-in organic cofactor directly coordinates to the copper ion through its phenolate moiety (Scheme 1) and serves as the one-electron redox center by shuttling between the phenolate and phenoxyl radical states during the enzymatic reactions (alcohol-oxidation and O_2-reduction).[3−5] Such a redox behavior of the organic cofactor was further supported by ESR studies[7] and by the mechanistic investigation using a mechanism-based inhibitor.[8]

Scheme 1

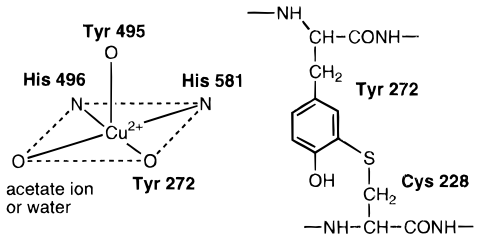

Thus, the active species (fully oxidized state) of the enzyme is a Cu(II)-phenoxyl radical that oxidizes alcohols formally in a two-electron plus two-proton process to generate the corresponding aldehydes and Cu(I)-phenolate species (fully reduced form, two protons are accommodated in other amino acid residues).[9] It is further proposed that the fully oxidized state is reproduced from the fully reduced state by reaction with molecular oxygen that is transformed into hydrogen peroxide as shown in eq 1. The interconversion between Cu(I) and Cu(II) states has also been demonstrated by X-ray absorption spectroscopy.[10] Very recently, such a phenoxyl radical−copper catalytic motif has also been found in glyoxal oxidase from *Phanerochaete chrysosporium*.[11]

One of the interesting features of this enzyme is the existence of the thioether linkage between Tyr 272 and Cys 228 (Scheme

† The Institute of Scientific and Industrial Research, Osaka University, Ibaraki, Osaka 567, Japan.

⊗ Abstract published in *Advance ACS Abstracts,* March 1, 1997.

(1) Amaral, D.; Kelly-Falcoz, F.; Horecker, B. L. *Methods Enzymol.* **1966**, *9*, 87. Tressel, P. S.; Kosman, D. J. *Methods Enzymol.* **1982**, *89*, 163.
(2) van der Meer, R. A.; Jongejan, J. A.; Duine, J. A. *J. Biol. Chem.* **1989**, *264*, 7792.
(3) Whittaker, M. M.; Whittaker, J. W. *J. Biol. Chem.* **1988**, *263*, 6074.
(4) Whittaker, M. M.; DeVito, V. L.; Asher, S. A.; Whittaker, J. W. *J. Biol. Chem.* **1989**, *264*, 7104.
(5) Whittaker, M. M.; Whittaker, J. W. *J. Biol. Chem.* **1990**, *265*, 9610.
(6) Ito, N.; Phillips, S. E. V.; Stevens, C.; Ogel, Z. B.; McPherson, M. J.; Keen, J. N.; Yadav, K. D. S.; Knowles, P. F. *Nature* **1991**, *350*, 87.
(7) (a) Babcock, G. T.; El-Deeb, M. K.; Sandusky, P. O.; Whittaker, M. M.; Whittaker, J. W. *J. Am. Chem. Soc.* **1992**, *114*, 3727. (b) Gerfen, G. J.; Bellew, B. F.; Griffin, R. G.; Singel, D. J.; Ekberg, C. A.; Whittaker, J. W. *J. Phys. Chem.* **1996**, *100*, 16739.
(8) Branchaud, B. P.; Montague-Smith, M. P.; Kosman, D. J.; McLaren, F. R. *J. Am. Chem. Soc.* **1993**, *115*, 798.
(9) Whittaker, M. M.; Whittaker, J. W. *Biophys. J.* **1993**, *64*, 762.
(10) Clark, K.; Penner-Hahn, J. E.; Whittaker, M. M.; Whittaker, J. W. *J. Am. Chem. Soc.* **1990**, *112*, 6433; *Biochemistry* **1994**, *33*, 12553.
(11) Whittaker, M. M.; Kersten, P. J.; Nakamura, N.; Sanders-Loehr, J.; Schweizer, E. S.; Whittaker, J. W. *J. Biol. Chem.* **1996**, *271*, 681.

S0020-1669(96)01144-5 CCC: $14.00

1). Then the question is why galactose oxidase and glyoxal oxidase employ such modified amino acid residues instead of a simple tyrosine. The redox potential of galactose oxidase is estimated to be 400−500 mV vs NHE,[5] which is significantly lower than that of free tyrosine in solution (930 mV) or tyrosine in enzymatic systems (760−1000 mV).[12,13] Such a negative shift of the redox potential has been attributed in part to the electron-donating nature of the thioether group[14] of the cofactor. On the other hand, Babcock and his co-workers reported that, in the radical state of the apoenzyme, about 25% of the spin density delocalizes into the sulfur atom of Cys 228, demonstrating the electron-sharing conjugative effect of the thioether group[14] of the cofactor.[7] Whittaker and his co-workers have recently reported the first synthetic models to provide information about the electronic structure of the cofactor and its interaction with the copper ion.[15−17] However, more comprehensive studies are desired for a complete understanding of the functions of the thioether group in each redox state of the cofactor and the copper complex. Thus, in this study, we synthesized a series of model compounds (**1H**−**4H**) and characterized not only the neutral, radical, and anionic states but also the copper complexes with and without the thioether group in order to obtain more detailed insight into the electronic effect of the substituent in the novel organic cofactor.[18]

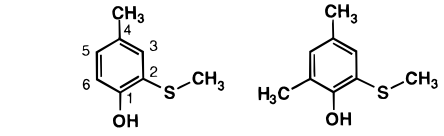

1H

2H

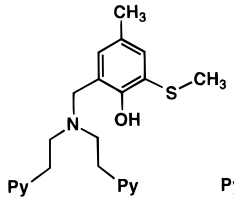

3H

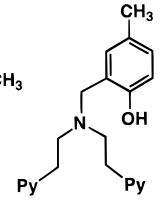

4H

Experimental Section

Reagents and solvents used in this study were commercial products of the highest available purity and were further purified by the standard methods.[19] Melting points were determined on a Yamato MP-21 apparatus and were uncorrected. IR spectra were recorded on a Hitachi 270-30 spectrophotometer and UV−vis spectra on a Shimadzu UV-265 spectrophotometer equipped with a Shimadzu TCC-260 thermostated cell holder or a Hewlett-Packard 8452A photodiode array spectrophotometer. ^{1}H NMR and ^{13}C NMR spectra were recorded on a JEOL FT-NMR EX-270 spectrometer.

ESR spectra were taken on a JEOL JES-ME-2X. The solution ESR spectrum of **1**• was measured under photolysis in the ESR cavity of a toluene solution containing **1H** (2.0 M) and dicumyl peroxide (1.0 M) at −30 °C. The solution ESR spectrum of **2**• was taken in a similar manner in benzene at room temperature. The *g* values were determined using a Mn^{2+} marker as a reference. Computer simulation of the ESR spectra were carried out by using ESRaII version 1.01 (Calleo Scientific Publisher) on a Macintosh personal computer.

Mass spectra were recorded on a JEOL JNX-DX303 HF mass spectrometer or a Shimadzu GCMS-QP2000 gas chromatograph mass spectrometer. A sector type mass spectrometer (JEOL-D300) connected with a homemade ESI (electrospray ionization) interface was used to obtain ESI mass spectra. The interface is similar to that of the ESI ion source designed by Fenn.[20] The sample solution was sprayed at the tip of a needle applied at a current 3.5 kV higher than that of the counter electrode. This electrode consisted of a 12-cm-long capillary pipe of stainless steel. A heated N_2 gas (70 °C) flowed between the needle and the capillary electrode to aid the desolvation of charged droplets sprayed. Ions entered the vacuum system through the first and the second skimmer to a mass spectrometer. The pressures of their region were about 10 and 0.1 Torr. The flow rate of a sample solution was 1−2 mL/min. In the present case, the ion translational energy was 2 kV. The voltage of the first skimmer was 50 V higher than that of the second, and that of the capillary electrode is 50 V higher than that of the first. For measurements of ESI mass spectra, all of the samples were dissolved in freshly distilled acetonitrile to prepare a sample concentration of ca. 0.1 mM.

The pulse radiolysis experiments were performed in an N_2O-saturated aqueous solution (pH 11) containing the phenol derivative (2×10^{-3} M) and NaN_3 (0.1 M) by referring to the reported method.[21] A sample solution was sealed in a $40 \times 10 \times 10$ mm^3 rectangular Suprasil cell. A transient absorption spectrum was measured at room temperature using a conventional nanosecond pulse radiolysis system consisting of an electron LINAC (energy, 28 MeV; pulse width, 8 ns; dose, 0.8 kGy/pulse), a Xe lamp (Osram, XBO-450), a monochrometer (CVI Laser, DIGIKROM-240), a photomultiplier tube (Hamamatsu, R-1477), a transient digitizer (Tektronix, 7912AD), and a microcomputer (Sharp, X-68000).

The second harmonic alternating current voltammetry (SHACV) and the cyclic voltammetry measurements were performed on a BAS 100B electrochemical analyzer in deaerated CH_3CN containing 0.10 M NBu_4ClO_4 as supporting electrolyte. The Pt and Au working electrodes (BAS) were polished with BAS polishing alumina suspension and rinsed with acetone before use. The counter electrode was a platinum wire. The measured potentials were recorded with respect to the $Ag/AgNO_3$ (0.01 M) reference electrode. The $E°_{red}$ and $E°_{ox}$ values (vs Ag/Ag^+) are converted to those vs SCE by adding 0.29 V.[22] All electrochemical measurements were carried out at 25 °C under an atmospheric pressure of nitrogen.

Molecular orbital calculations were performed with the MOPAC program (version 6) by using a CAChe Work System (SONY Tektronix) and a MOL-GRAPH program (version 2.8 supplied by Daikin Industries, Ltd.).[23] Final geometries and energetics were obtained by optimizing the total molecular energy with respect to all structural variables.

(12) Harriman, A. *J. Phys. Chem.* **1987**, *91*, 6102.
(13) Boussac, A.; Eteinne, A. L. *Biochim. Biophys. Acta* **1984**, *766*, 576.
(14) Tagaki, W. In *Organic Chemistry of Sulfur*; Oae, S., Ed.; Plenum Press: New York, 1977; Chapter 6, pp 231−302
(15) Whittaker, M. M.; Chuang, Y.-Y.; Whittaker, J. W. *J. Am. Chem. Soc.* **1993**, *115*, 10029.
(16) Whittaker, M. M.; Duncan, W. R.; Whittaker, J. W. *Inorg. Chem.* **1996**, *35*, 382.
(17) Copper (II) complexes having a simple phenol moiety have been reported: (a) Karlin, K. D.; Cohen, B. I. *Inorg. Chim. Acta* **1985**, *107*, L17. (b) Karlin, K. D.; Cohen, B. I.; Hayes, J. C.; Farooq, A.; Zubieta, J. *Inorg. Chem.* **1987**, *26*, 147. (c) Rajendran, U.; Viswanathan, R.; Palaniandavar, M.; Lakshminarayanan, M. *J. Chem. Soc., Dalton Trans.* **1992**, 3563. (d) Uma, R.; Viswanathan, R.; Palaniandavar, M.; Lakshminarayanan, M. *J. Chem. Soc., Dalton Trans.* **1994**, 1219. (e) Adams, H.; Bailey, N. A.; Febton, D. E.; He, Q.; Ohba, M.; Okawa, H. *Inorg. Chim. Acta* **1994**, *215*, 1. (f) Adams, H.; Bailey, N. A.; Rodriguez de Barbarin, C. O.; Fenton, D. E.; He, Q.-Y. *J. Chem. Soc., Dalton Trans.* **1995**, 2323. (g) Adams, H.; Bailey, N. A.; Campbell, I. K.; Fenton, D. E.; He, Q.-Y. *J. Chem. Soc., Dalton Trans.* **1996**, 2233.
(18) Preliminary results have already been reported: Itoh, S.; Hirano, K.; Furuta, A.; Komatsu, M.; Ohshiro, Y.; Ishida, A.; Takamuku, S.; Kohzuma, T.; Nakamura, N.; Suzuki, S. *Chem. Lett.* **1993**, 2099.
(19) Perrin, D. D.; Armarego, W. L. F.; Perrin, D. R. *Purification of Laboratory Chemicals*; Pergamon Press: Elmsford, NY, 1966.
(20) Whitehouse, C. M.; Dreyer, R. N.; Yamasita, M.; Fenn, J. B. *Anal. Chem.* **1985**, *57*, 675.
(21) Lind, J.; Shen, X.; Eriksen, T. E.; Merényi, G. *J. Am. Chem. Soc.* **1990**, *112*, 479.
(22) Mann, C. K.; Barnes, K. K. *Electrochemical Reactions in Non-aqueous Systems*; Marcel Deker, Inc.: New York, 1990.
(23) The PM3 method: Stewart, J. J. P. *J. Comput. Chem.* **1989**, *10*, 209, 221.

Syntheses. Model compounds **1H** (2-methylthio-*p*-cresol) and **2H** (2-methylthio-4,6-dimethylphenol) were prepared from *p*-cresol and 2,4-dimethylphenol according to the reported procedure, respectively.[24] The structures were confirmed by the following analytical data.

1H (yellow oil): IR (neat) 3468 cm^{-1} (OH); ^1H NMR ($CDCl_3$) δ 2.26 (3 H, s, CH_3), 2.32 (3 H, s, SCH_3), 6.46 (1 H, s, OH), 6.87 (1 H, d, J = 8.3 Hz, H-6), 7.05 (1 H, dd, J = 2.1, 8.3 Hz, H-5), 7.28 (1 H, d, J = 2.1 Hz, H-3); ^{13}C NMR ($CDCl_3$) 19.9 (CH_3), 20.3 (CH_3), 111.5, 120.5, 130.2, 131.4, 134.9, 154.0 ppm (six aromatic carbons); MS (EI) *m/z* 154 (M^+); UV−vis (CH_3CN) λ_{max} = 250 (ϵ = 4330 M^{-1} cm^{-1}), 295 nm (3720).

2H (yellow oil): IR (neat) 3470 cm^{-1} (OH); ^1H NMR ($CDCl_3$) δ 2.23 (3 H, s, CH_3), 2.24 (3 H, s, CH_3), 2.31 (3 H, s, SCH_3), 6.59 (1 H, s, OH), 6.92 (1 H, s, H-5), 7.13 (1 H, s, H-3); ^{13}C NMR ($CDCl_3$) 16.0 (CH_3), 19.3 (CH_3), 19.9 (CH_3), 119.5, 123.5, 128.8, 131.9, 132.3, 152.0 ppm (six aromatic carbons); MS (EI) *m/z* 168 (M^+); UV−vis (CH_3CN) λ_{max} = 252 (ϵ = 3620 M^{-1} cm^{-1}), 292 nm (3940).

2-(Methylthio)-4-methyl-6-[[bis[2-(2-pyridyl)ethyl]amino]methyl]-phenol (**3H**). To a suspension of paraformaldehyde (0.02 mol) in ethanol (50 mL) were added bis[2-(2-pyridyl)ethyl]amine[25] (0.015 mol) and **1H** (0.015 mol), and the mixture was refluxed for 48 h under N_2. Removal of the solvent gave a brown residue from which **3H** was isolated in 31% yield by column chromatography (SiO_2, $CHCl_3$−CH_3OH): IR (neat) 2930 cm^{-1} (OH); ^1H NMR ($CDCl_3$) δ 2.23 (3 H, s, CH_3), 2.41 (3 H, s, SCH_3), 3.03 (8 H, m, ethylene protons), 3.84 (2 H, s, methylene protons), 6.60 (1 H, s, H-5), 6.89 (1 H, s, H-3), 7.11 (2 H, ddd, J = 1.8, 5.9, 8.1 Hz, H-5′ on the pyridine nuclei), 7.15 (2 H, dd, J = 1.8, 8.1 Hz, H-3′ on the pyridine nuclei), 7.58 (2 H, dt, J = 2.4, 8.1 Hz, H-4′ on the pyridine nuclei), 8.49 (2 H, dd, J = 2.4, 5.9 Hz, H-6′ on the pyridine nuclei); ^{13}C NMR ($CDCl_3$) 15.2 (CH_3), 20.6 (SCH_3), 35.0, 53.2, 57.9 (three methylene carbons), 121.0, 121.4, 123.4, 124.2, 126.5, 126.9, 128.5, 136.5, 149.3, 152.9, 159.4 ppm (eleven aromatic carbons); high-resolution MS, *m/z* 393.1859 (M^+) calcd for $C_{23}H_{27}ON_3S$ 393.1877; UV−vis (CH_3CN) λ_{max} = 255 (ϵ = 10 800 M^{-1} cm^{-1}), 298 nm (4070).

2-[[Bis[2-(2-pyridyl)ethyl]amino]methyl]-4-methylphenol (**4H**) was prepared in a similar manner to that described above and isolated in 40% yield by column chromatography (SiO_2, $CHCl_3$−CH_3OH): IR (neat) 2930 cm^{-1} (OH); ^1H NMR ($CDCl_3$) δ 2.20 (3 H, s, CH_3), 2.92−3.12 (8 H, m, ethylene protons), 3.84 (2 H, s, methylene protons), 6.64 (1 H, d, J = 8.3 Hz, H-2), 6.76 (1 H, d, J = 2.7 Hz, H-5), 6.93 (1 H, dd, J = 2.7, 8.3 Hz, H-3), 7.04−7.19 (4 H, m, H-3′ and H-5′ on the pyridine nuclei), 7.56 (2 H, dt, J = 1.9, 7.7 Hz, H-4′ on the pyridine nuclei), 8.50 (2 H, dd, J = 1.9, 4.6 Hz, H-6′ on the pyridine nuclei); ^{13}C NMR ($CDCl_3$) 20.6 (SCH_3), 34.6, 52.8, 57.6 (three methylene carbons), 111.5, 121.1, 121.3, 123.0, 127.6, 128.7, 128.9, 136.1, 148.9, 155.0, 159.1 ppm (eleven aromatic carbons); high-resolution MS, *m/z* 347.2006 (M^+) calcd for $C_{22}H_{25}ON_3$ 347.1997; UV−vis (CH_3CN) λ_{max} = 262 (ϵ = 6620 M^{-1} cm^{-1}), 290 nm (shoulder).

$[Cu^{II}_2(3^-)_2](PF_6)_2$ (Dimer Complex 7). To a solution of ligand **3H** (0.48 mmol) and triethylamine (0.50 mmol) in methanol (3.0 mL) was added $CuCl_2 \cdot 2H_2O$ (0.48 mmol) in methanol (1.0 mL), and the mixture was refluxed for 2 h. $NaPF_6$ (0.96 mmol) suspended in methanol (2.0 mL) was then added into the dark violet solution, and the mixture was stirred for an additional 1 h. The solution was then poured into water (100 mL) to provide a dark violet solid that was collected by filtration, washed with water, and dried in vacuo, 82.1% yield. Single crystals (dark violet prism) for X-ray structure determination were obtained by recrystallization from H_2O−CH_3CN. Anal. Calcd for $[Cu^{II}_2(3^-)_2](PF_6)_2 \cdot H_2O$, $C_{46}H_{54}O_3N_6S_2P_2F_{12}Cu_2$: C, 45.28; H, 4.46; N, 6.89. Found: C, 45.20, H, 4.24, N, 6.84.

$[Cu^{II}_2(4^-)_2](PF_6)_2$ (**dimer complex 8**) was synthesized in 91.2% yield, according to the same procedure as described above. Single crystals (dark brown prism) for X-ray structure determination were obtained by recrystallization from CH_3CN. Anal. Calcd for $[Cu^{II}_2(4^-)_2](PF_6)_2$, $C_{44}H_{48}O_2N_6P_2F_{12}Cu_2$: C, 47.61; H, 4.36; N, 7.57. Found: C, 47.36; H, 4.39; N, 7.29.

X-ray Structure Determination of Dimer Copper(II) Complexes 7 and 8. All the X-ray experiments were carried out on a Rigaku AFC-5R diffractometer with graphite-monochromated Mo Kα radiation and a rotating anode generator. Since single crystals of **7** and **8** were not sufficiently stable against dryness, the intensity measurement was undertaken by sealing them in glass capillary tubes containing the mother liquid. The absorption effect was corrected empirically on the basis of azimuthal scans of three reflections. The crystal structures were solved by Patterson methods and refined by full-matrix least-squares techniques. The non-hydrogen atoms were refined anisotropically, while the hydrogen atoms located from the final stage of difference Fourier maps were included with isotropic thermal parameters. All the calculations were performed by using the TEXSAN program package.[26] Summaries of the fundamental crystal data and experimental parameters for structure determinations are given in Table 3. Atomic coordinates, thermal parameters, and intramolecular bond distances and angles have been deposited in the Supporting Information.

Table 1. Selected Physicochemical Data of **1H**, **2H**, **3H**, **4H**, and *p*-Cresol (**5H**) and Their Anionic Forms

	^1H NMR/δ[a]						
compd	H-3	H-5	OH	UV−vis[b] λ_{max}/nm		pK_a[c]	$E°_{ox}$ vs SCE[d]
1H	7.12	6.91	6.87	250	295	9.6	+1106
2H	7.07	6.89	6.62	252	292	9.9	+955
3H	6.86	6.63	*e*	255	298	12.0	+355
4H	6.91	6.81	*e*	262	290[f]	12.1	+538
5H	7.00	7.00	6.66	223	280	10.4	+1474
$\mathbf{1}^-$	6.65	6.57		268[f]	338		−246
$\mathbf{2}^-$	6.53	6.52		270[f]	334		−326
$\mathbf{3}^-$	6.52	6.51		270[f]	341		−314
$\mathbf{4}^-$	6.58	6.68		256	327		−273
$\mathbf{5}^-$	6.72	6.72		251	321		−146

[a] 50 mM in CD_3CN; the phenolate form was generated in the NMR tube by adding 4 equiv of NMe_4OH. [b] In CH_3CN; the phenolate form was generated in the UV cell by adding 10-fold excess of NMe_4OH. [c] Determined by ordinary photometric titration in 0.1 M aqueous buffer solution containing 1% CH_3OH. [d] One-electron oxidation potential determined by SHACV method in CH_3CN containing 0.1 M NBu_4ClO_4; the anionic form was generated in the cell by adding a slight excess of NMe_4OH. [e] Not detected because of the significant broadening. [f] Shoulder.

Results and Discussion

Characterization of Organic Cofactor Models. Selected analytical data of cofactor models **1H**, **2H**, and **3H** are summarized in Table 1 together with those of **4H** and *p*-cresol (**5H**) for comparison. Judging from the chemical shifts (δ in the ^1H NMR) of the aromatic protons at the 3- and 5-positions, the substituent effect of the methylthio group on the ^1H NMR chemical shift is not so significant in both the neutral and anionic forms; the differences in $\Delta\delta$ of the corresponding protons between **1H** and **5H**, **3H** and **4H**, $\mathbf{1}^-$ and $\mathbf{5}^-$, and $\mathbf{3}^-$ and $\mathbf{4}^-$ are within ca. 0.1. In general, however, introduction of a methylthio group into the 2-position causes up-field shifts of the aromatic protons, indicating that the substituent has an electron-donating nature.[14]

Compound **1H** shows a pH-dependent UV−vis spectral change due to the acid−base equilibrium of the phenol proton in aqueous buffer solutions;[15] the absorption at 291 nm due to **1H** decreases with an increase in the absorption at 311 nm due to $\mathbf{1}^-$ with a clear isosbestic point at 297 nm as the pH of the solution is raised. The pK_a of the phenol proton was determined to be 9.6 by nonlinear curve fitting of the absorbance change using the equation $A = (\epsilon_{\mathbf{1H}}K_a[H^+] + \epsilon_{\mathbf{1}^-})[\mathbf{1H}]_T/(K_a[H^+] + 1)$, where $\epsilon_{\mathbf{1H}}$ and $\epsilon_{\mathbf{1}^-}$ are the molar absorption coefficients of **1H** and $\mathbf{1}^-$, respectively, and $[\mathbf{1H}]_T$ is a total concentration of **1H** used for the titration (Figure 1).

(24) Farah, B. S.; Gilbert, E. E. *J. Org. Chem.* **1963**, *28*, 2807.
(25) Romary, J. K.; Zachariasen, R. D.; Barger, J. D.; Schiesser, H. *J. Chem. Soc. C* **1968**, 2884.
(26) *TEXSAN, Single Crystal Structure Analysis Software*, Version 5.0, Molecular Structure Corp., The Woodlands, TX 77381, 1989.

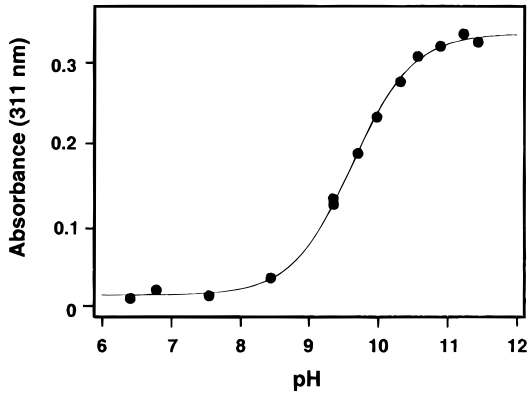

Figure 1. Spectrophotometric titration of **1H** (5×10^{-5} M) in a 0.1 M buffer solution containing 1% CH_3OH. The solid line is generated by the nonlinear curve fitting using the equation $A = (\epsilon_{\mathbf{1H}}K_a[H^+] + \epsilon_{\mathbf{1}^-})[\mathbf{1H}]_T/(K_a[H^+] + 1)$.

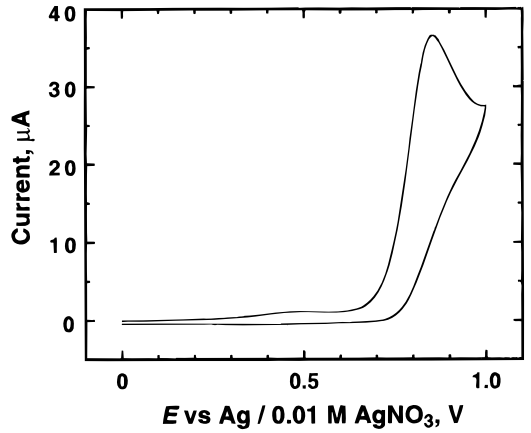

Figure 2. Cyclic voltammogram for the oxidation of **1H** (5×10^{-3} M) in deaerated acetonitrile containing 0.1 M NBu_4ClO_4 with a Pt working electrode; sweep rate 100 mV s^{-1}.

The pK_a values of the phenolic protons of other model compounds were determined in a similar manner and are also listed in Table 1. Introduction of a methylthio group into the ortho position causes an increase in the acidity of the phenol proton by about 1 pH unit (**1H**, 9.6; **5H**, 10.4). A decrease of the pK_a value of *p*-alkylthio-substituted phenols as compared to that of phenol itself was also reported,[27] and such a phenomenon has been explained by taking account of the fact that the sulfide group can stabilize negative charge when connected with a conjugated system, so-called $2p\pi-3d\pi$ conjugation.[14] The PM3 calculations supported such a possibility; net atomic charges of the sulfur atoms in **1H** and $\mathbf{1}^-$ are +0.064 and −0.04, respectively. On the other hand, much higher pK_as of **3H** and **4H** are due to the existence of strong hydrogen bonding between the phenol proton and the nitrogen atoms of the pyridine groups and the tertiary amine group of the ligand, and such strong hydrogen bonding may obscure the electronic effect of the methylthio substituent (ΔpK_a between **3H** and **4H** is only 0.1).

All the phenol derivatives gave irreversible cyclic voltammograms. This is due to the instability of the corresponding phenoxyl radicals in solution. In Figure 2 is shown an irreversible cyclic voltammogram of **1H** in CH_3CN as a representative example.[16] The SHACV method is known to provide a superior approach to the direct evaluation of the one-electron redox potentials in the presence of a follow-up chemical reaction.[28] A well-defined symmetrical SHACV trace was obtained for the one-electron oxidation of **1H** in CH_3CN as shown in Figure 3, in which the intersection with the dc potential axis corresponds to the one-electron oxidation potential ($E°_{ox}$). The $E°_{ox}$ of other phenol derivatives and the corresponding deprotonated forms (tetramethylammonium salts of the phenolate derivatives) were determined by the SHACV method in a similar manner and are listed in Table 1 (the $E°_{ox}$ values (vs Ag/0.01 M Ag^+) are converted to those vs SCE by adding 0.29 V[22]). Introduction of a methylthio group into the ortho position of the phenol ring causes a negative shift of $E°_{ox}$ by hundreds of millivolts (see Table 1). The substituent effect of a methylthio group on the redox potential is discussed below in detail.

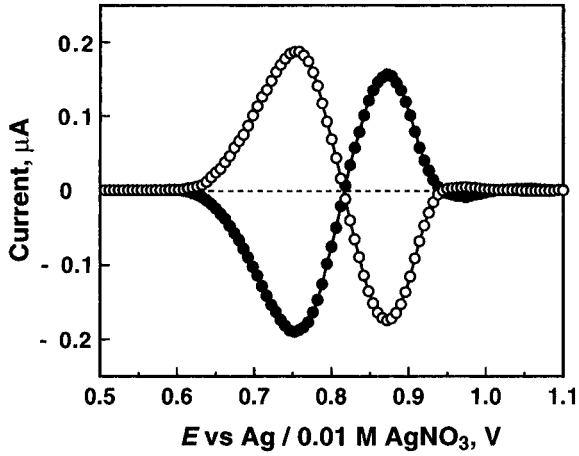

Figure 3. Second harmonic ac voltammogram of **1H** (5×10^{-3} M) in deaerated acetonitrile containing 0.1 M NBu_4ClO_4 with a Pt working electrode; sweep rate 4 mV s^{-1}, ac amplitude 25 mV, ac frequency 50 Hz, and phase shift 178/268°.

Phenoxyl Radicals. Characterization of radical species of the model compounds is worthwhile, since the phenoxyl radical of the cofactor has been demonstrated to be the oxidation active species in the enzymatic reaction.[3−5] Absorption spectra of the radical species of compound **1H** and *p*-cresol (**5H**) were obtained by the pulse radiolysis in an alkaline aqueous solution (Figure 4). *p*-Cresol shows a characteristic absorption at around 400 nm due to the phenoxyl radical.[29] On the other hand, model compound **1H** gave a very broad absorption from 600 to 900 nm together with strong ones at around 350 and 400 nm. The absorption spectrum of $\mathbf{1}^\bullet$ in solution is very close to that of the oxidized apogalactose oxidase,[5] indicating that compound **1H** is a good model of the active site cofactor of apogalactose oxidase. Whittaker and his co-workers obtained essentially the same spectrum of $\mathbf{1}^\bullet$ by UV irradiation in a propionitrile−butyronitrile matrix at 77 K.[15]

Well-resolved solution ESR spectra of $\mathbf{1}^\bullet$ and $\mathbf{2}^\bullet$ were obtained under photolysis in the ESR cavity of a solution of **1H** or **2H** containing dicumyl peroxide at ambient temperature.[30] In Figure 5 are shown the solution ESR spectra of $\mathbf{1}^\bullet$ and $\mathbf{2}^\bullet$ [A and C] together with the computer simulation spectra [B and D]. The *g* values of $\mathbf{1}^\bullet$ and $\mathbf{2}^\bullet$ are determined to be 2.0060 and 2.0052 using an Mn^{2+} marker as reference, respectively, which are very close to that of the cofactor radical (2.0055) in the enzyme active

(27) Oae, S.; Yoshihara, M.; Tagaki, W. *Bull. Chem. Soc. Jpn.* **1967**, *40*, 951.

(28) (a) McCord, T. G.; Smith, D. E. *Anal. Chem.* **1969**, *41*, 1423. (b) Bond, A. M.; Smith, D. E. *Anal. Chem.* **1974**, *46*, 1956. (c) Wasielewski, M. R.; Breslow, R. *J. Am. Chem. Soc.* **1976**, *98*, 4222. (d) Arnett, E. M.; Amarnath, K.; Harvey, N. G.; Cheng, J.-P. *J. Am. Chem. Soc.* **1990**, *112*, 344. (e) Fukuzumi, S.; Fujita, M.; Maruta, J.; Chanon, M. *J. Chem. Soc., Perkin Trans. 2* **1994**, 1597.

(29) Tripathi, G. N. R.; Schuler, R. H. *J. Phys. Chem.* **1988**, *92*, 5129.

(30) Krusic, P. J.; Kochi, J. K. *J. Am. Chem. Soc.* **1968**, *90*, 7155.

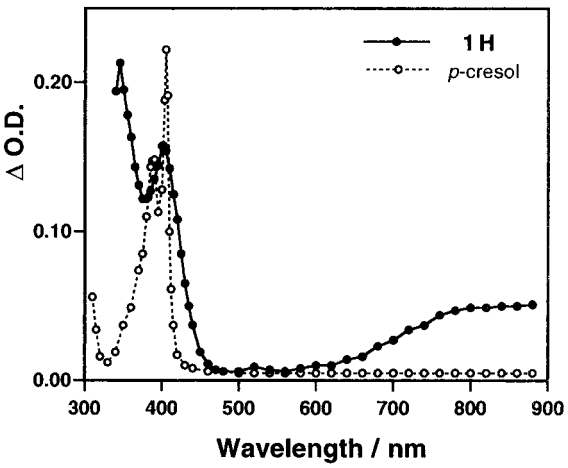

Figure 4. Transient absorption spectra obtained by the pulse radiolysis of **1H** and *p*-cresol in an N_2O-saturated aqueous solution (pH 11) containing NaN_3 (0.1 M).

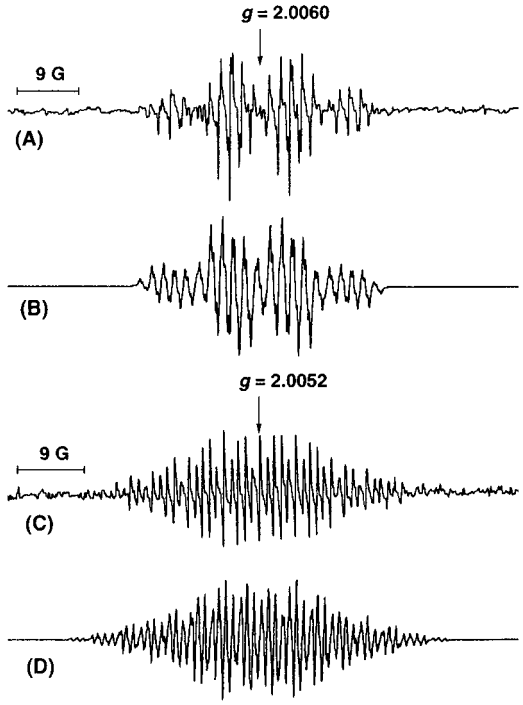

Figure 5. (A) Solution ESR spectrum of **1**• obtained under photolysis in the ESR cavity of a toluene solution of **1H** (2.0 M) containing 1.0 M dicumyl peroxide at −30 °C; microwave frequency 9.09 GHz, modulation frequency 100 kHz, modulation amplitude 0.5 G, microwave power 8 mW. (B) Computer simulation spectrum for **1**• using the parameters (*g* and hfc values) listed in Table 2. (C) Solution ESR spectrum of **2**• obtained under photolysis in the ESR cavity of a benzene solution of **2H** (2.0 M) containing 1.0 M dicumyl peroxide at 25 °C; microwave frequency 9.45 GHz, modulation frequency 100 kHz, modulation amplitude 0.5 G, microwave power 8 mW. (D) Computer simulation spectrum for **2**• using the parameters (*g* and hfc values) listed in Table 2.

site but significantly larger than that of the phenoxyl radicals of 2,4,6-trimethylphenol (**6H**) (2.0036) (see Table 2). Thus, the larger *g* values of the cofactor models can be attributed to the electronic effect of the sulfur atom which has a larger spin−orbital coupling constant.

Hyperfine coupling constants (hfc) determined by the computer simulation for **1**• and **2**• are listed in Table 2 together with those of phenoxyl radicals of *p*-cresol (**5**•) and 2,4,6-trimethylphenol (**6**•). The isotropic hfc values for **1**• in solution agree with those estimated from the reported anisotropic hfc values obtained from the powder ESR spectrum.[7] It is obvious that

Table 2. Isotopic *g* Values and Proton Hyperfine Coupling Constants (G) for the Phenoxyl Radicals

radical	*g*	A_2	A_{3-H}	A_{4-Me}	A_{5-H}	A_6
1• [a]	2.0060	1.7[e]	0.3	8.6	0.5	3.1[h]
5• [b]	[d]	6.1[f]	1.4	12.3	1.4	6.1[h]
2• [c]	2.0052	2.8[e]	0.7	9.6	0.9	3.9[i]
6• [c]	2.0036	6.2[g]	1.6	11.2	1.6	6.2[i]

[a] [**1H**] = 2.0 M, [dicumyl peroxide] = 1.0 M, at −30 °C, in toluene. [b] Taken from the following: Dixon, W. T.; Norman, R. O. C. *J. Chem. Soc.* **1964**, 4857. [c] [compd] = 2.0 M, [dicumyl peroxide] = 1.0 M, at 25 °C, in benzene. [d] Not reported. [e] For 2-SCH_3. [f] For 2-H. [g] For 2-CH_3 [h] For 6-H. [i] For 6-CH_3.

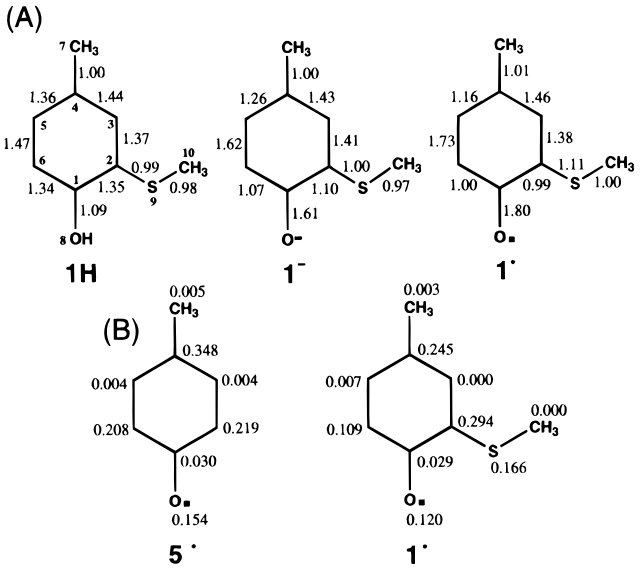

Figure 6. (A) Bond orders of **1H**, **1**⁻, and **1**• calculated by the PM3 method. (B) Spin densities of **5**• and **1**• calculated by the PM3 method.

Scheme 2

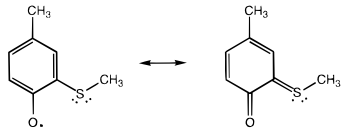

the total spin density at the 3-, 4-, 5-, and 6-positions in **1**• and **2**• decreases by about 41% and 26% as compared to that of **5**• and **6**•, respectively. These results indicate that a relatively large amount of the spin density delocalizes into the sulfur atom of the methylthio group.

Semiempirical molecular orbital calculations (PM3)[22] on compound **1H** and its anionic (**1**⁻) and radical (**1**•) species reveal the electronic effect more clearly. Figure 6, part A, shows the bond orders in the optimized structures of **1H**, **1**⁻, and **1**•. The bond orders of C(1)−O(8), C(5)−C(6), and C(2)−S(9) increase in going from **1H** to **1**•, while those of C(1)−C(2), C(4)−C(5), and C(1)−C(6) decrease. These results indicate that the *o*-quinonoid canonical form (Scheme 2) partially contributes to the stabilization of the radical species, though the bond-order changes of C(2)−C(3) and C(3)−C(4) are very small. Calculated spin density of **1**• is compared with that of the phenoxyl radical of *p*-cresol (**5**•) in Figure 6, part B. The spin densities at C(4), C(6), and O(8) are diminished by introduction of a methylthio substituent into the 2-position of *p*-cresol, while the unpaired electron is distributed between C(2) and S(9) to a considerable extent. These results are consistent with the well-documented electron-sharing conjugative effect of sulfide groups (Scheme 2).[14]

It is also interesting to note that, in the optimized molecular geometry of **1**•, the methylthio group stays in the same plane of

Table 3. Summary of X-ray Crystallographic Data

compound	$[Cu^{II}_2(\mathbf{3}^-)_2](PF_6)_2\cdot 2CH_3CN$ (**7**)	$[Cu^{II}_2(\mathbf{4}^-)_2](PF_6)_2$ (**8**)
empirical formula	$C_{50}H_{58}F_{12}Cu_2N_8O_2P_2S_2$	$C_{44}H_{48}F_{12}Cu_2N_6O_2P_2$
formula weight	1284.20	1109.92
crystal system	triclinic	monoclinic
space group	$P\bar{1}$ (No. 2)	$P2_1/c$ (No. 14)
a, Å	14.394(3)	17.845(3)
b, Å	17.587(6)	13.005(4)
c, Å	13.027(5)	20.307(3)
α, deg	103.82(3)	
β, deg	111.02(2)	91.94(1)
γ, deg	92.40(2)	
V, Å^3	2959(1)	4710(1)
Z	2	4
F(000)	2456.00	2048.00
D_{calc}, g/cm^3	1.441	1.565
T, °C	23	23
crystal size, mm	0.40 × 0.30 × 0.30	0.50 × 0.50 × 0.20
μ (Mo Kα), cm^{-1}	18.30	10.35
diffractometer	Rigaku AFC5R	Rigaku AFC5R
radiation	Mo Kα (0.71069 Å)	Mo Kα (0.71069 Å)
scan type	$\omega-2\theta$	$\omega-2\theta$
$2\theta_{max}$, deg	55.1	55.1
scan width, deg	1.21 + 0.35 tanθ	0.89 + 0.35 tanθ
scan rate in ω, deg/min	10.0	10.0
no. of reflcns measd	14211	11732
no. of reflcns obsd [$I > 3\sigma(I)$]	7432	4108
no. of variables	935	805
R	0.075	0.076

the aromatic ring, while the methyl group moves away from the plane in **1H** and **1**$^-$. The dihedral angles defined by C(1)−C(2)−S(9)−C(10) in **1H** and **1**$^-$ are 70° and 60°, respectively. The difference in the optimized structure between **1**$^\bullet$ and **1H** or **1**$^-$ suggests the increasing sp^2 character of the sulfur atom in the radical state, also implying the contribution of the *o*-quinonoid canonical form as illustrated in Scheme 2. The partial double-bond character of the thioether linkage in the native cofactor was also suggested by its similar molecular geometry in the enzyme active site.[6] Thus, the relatively large negative shift of the $E°_{ox}$ values of the model compounds having a methylthio group as compared to the corresponding phenol derivatives without the substituent (Table 1) can be attributed to both the electron-donating nature and the radical-stabilizing effect by electron spin delocalization into the methylthio group, so-called electron-sharing conjugative effect.

The SOMO and LUMO of **1**$^\bullet$ were also calculated by the PM3 method (see Supporting Information). The SOMO orbital is located mainly on the benzene ring [C(2), C(4), and C(6)], while the LUMO orbital is just sitting around the methylthio group. Thus, the very broad absorbance of **1**$^\bullet$ in Figure 4 could be attributed to intramolecular charge transfer from the benzene ring to the methylthio group.

Copper Complexes. Model copper(II) complexes of **3H** and **4H** were prepared in order to shed light on the substituent effect on the copper ion center. Addition of $CuCl_2\cdot 2H_2O$ to deprotonated ligand **3**$^-$ in methanol leads to formation of dimeric complex **7** that immediately crystallized when $NaPF_6$ was added into the solution. Single crystals (dark violet prism) of **7** for X-ray structure determination were obtained by recrystallization from H_2O-CH_3CN. The copper(II) complex of **4**$^-$ (dimer complex **8**) was synthesized in a similar manner, and single crystals (dark brown prism) for the X-ray crystallographic analysis were obtained by recrystallization from CH_3OH. Crystallographic data and selected bond distances and angles for the X-ray structures of the dinuclear copper(II) complexes **7** and **8** are summarized in Tables 3 and 4, respectively, with ORTEP drawings shown in Figures 7 and 8.

Table 4. Selected Bond Lengths (Å) and Angles (deg) for **7** and **8**[a]

$[Cu^{II}_2(\mathbf{3}^-)_2](PF_6)_2\cdot 2CH_3CN$ (**7**)			
Cu(1)−O(1)	1.955(7)	Cu(1)−O(2)	2.025(7)
Cu(1)−N(1)	2.270(10)	Cu(1)−N(2)	2.023(10)
Cu(1)−N(3)	1.990(10)	Cu(2)−O(1)	2.096(7)
Cu(2)−O(2)	1.913(7)	Cu(2)−N(4)	2.122(9)
Cu(2)−N(5)	1.97(1)	Cu(2)−N(6)	2.167(10)
S(1)−C(6)	1.75(1)	S(1)−C(8)	1.79(2)
S(2)−C(29)	1.76(1)	S(2)−C(31)	1.79(2)
O(1)−Cu(1)−O(2)	74.4(3)	O(1)−Cu(1)−N(1)	90.9(3)
O(1)−Cu(1)−N(2)	97.1(3)	O(1)−Cu(1)−N(3)	167.3(4)
O(2)−Cu(1)−N(1)	117.3(3)	O(2)−Cu(1)−N(2)	146.4(4)
O(2)−Cu(1)−N(3)	94.2(3)	N(1)−Cu(1)−N(2)	94.9(4)
N(1)−Cu(1)−N(3)	89.5(4)	N(2)−Cu(1)−N(3)	95.5(4)
O(1)−Cu(2)−O(2)	73.6(3)	O(1)−Cu(2)−N(4)	155.7(3)
O(1)−Cu(2)−N(5)	93.0(3)	O(1)−Cu(2)−N(6)	105.8(3)
O(2)−Cu(2)−N(4)	92.3(3)	O(2)−Cu(2)−N(5)	159.1(4)
O(2)−Cu(2)−N(6)	97.4(3)	N(4)−Cu(2)−N(5)	94.3(4)
N(4)−Cu(2)−N(6)	95.3(4)	N(5)−Cu(2)−N(6)	101.7(4)
Cu(1)−O(1)−Cu(2)	102.3(3)	Cu(1)−O(2)−Cu(2)	106.5(3)
C(6)−S(1)−C(8)	101.5(10)	C(29)−S(2)−C(31)	102.4(8)
$[Cu^{II}_2(\mathbf{4}^-)_2](PF_6)_2$ (**8**)			
Cu(1)−O(1)	1.920(8)	Cu(1)−O(2)	2.021(7)
Cu(1)−N(1)	2.259(10)	Cu(1)−N(2)	2.04(1)
Cu(1)−N(3)	1.96(1)	Cu(2)−O(1)	2.017(8)
Cu(2)−O(2)	1.926(8)	Cu(2)−N(4)	2.12(1)
Cu(2)−N(5)	1.96(1)	Cu(2)−N(6)	2.14(1)
O(1)−Cu(1)−O(2)	74.2(3)	O(1)−Cu(1)−N(1)	92.9(3)
O(1)−Cu(1)−N(2)	92.4(4)	O(1)−Cu(1)−N(3)	167.5(4)
O(2)−Cu(1)−N(1)	116.0(3)	O(2)−Cu(1)−N(2)	147.9(4)
O(2)−Cu(1)−N(3)	93.3(4)	N(1)−Cu(1)−N(2)	93.3(4)
N(1)−Cu(1)−N(3)	91.6(4)	N(2)−Cu(1)−N(3)	99.0(4)
O(1)−Cu(2)−O(2)	74.2(3)	O(1)−Cu(2)−N(4)	152.6(3)
O(1)−Cu(2)−N(5)	92.3(4)	O(1)−Cu(2)−N(6)	109.9(3)
O(2)−Cu(2)−N(4)	94.8(4)	O(2)−Cu(2)−N(5)	164.3(4)
O(2)−Cu(2)−N(6)	94.4(4)	N(4)−Cu(2)−N(5)	93.7(4)
N(4)−Cu(2)−N(6)	95.7(4)	N(5)−Cu(2)−N(6)	97.9(4)
Cu(1)−O(1)−Cu(2)	105.6(4)	Cu(1)−O(2)−Cu(2)	105.2(4)

[a] Estimated standard deviations are given in parentheses.

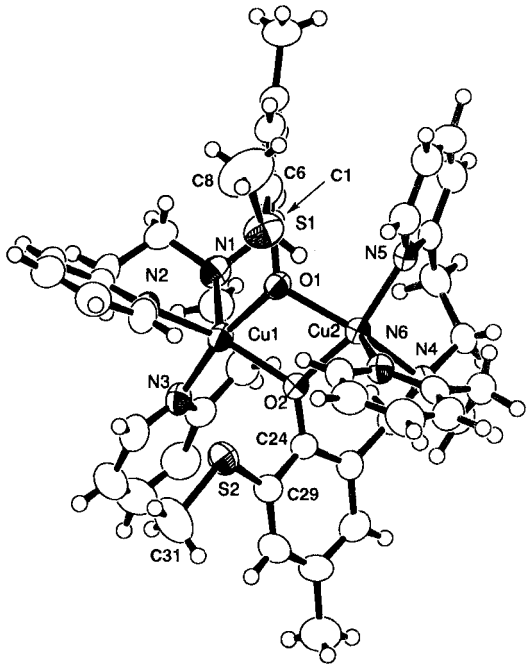

Figure 7. ORTEP drawing of $[Cu^{II}_2(\mathbf{3}^-)_2](PF_6)_2$ (**7**).

Complex **7** has two nonequivalent five-coordinated metal ion centers as indicated in Figure 7. Each metal ion is coordinated by two pyridine nitrogen atoms, the tertiary amine nitrogen atom, and two phenolate oxygen atoms which also coordinate to another copper ion in the dimer complex, but there is no coordinative interaction between Cu(II) and the sulfur atoms

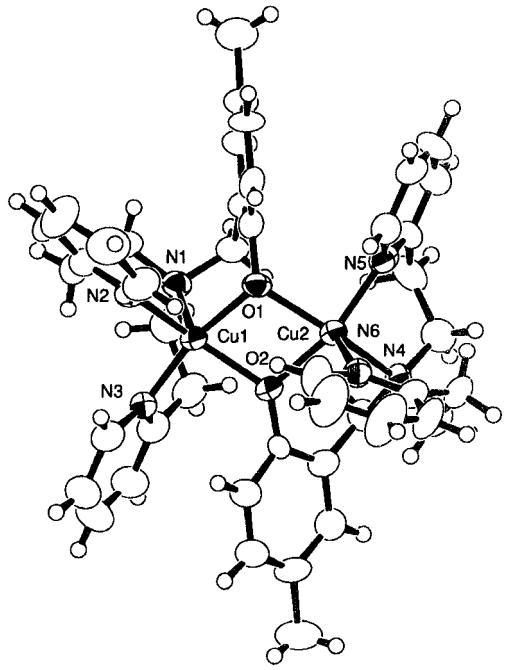

Figure 8. ORTEP drawing of $[Cu^{II}_2(\mathbf{4}^-)_2](PF_6)_2$ (**8**).

of the methylthio groups as in the case of the enzymatic system[6] (the distances for Cu(1)−S(1), Cu(1)−S(2), Cu(2)−S(1), and Cu(2)−S(2) are 4.35, 3.29, 4.22, and 4.32 Å, respectively). The copper−copper separation is 3.16 Å. The geometries at the Cu(1) and Cu(2) centers can be described as distorted square pyramidal. The relative amounts of the trigonal-bipyramidal component are indicated by an index τ representing the degree of trigonality within the structural continuum between square-planar and trigonal-bipyramidal geometries. The τ values the at the Cu(1) and Cu(2) centers are obtained as 0.348 and 0.057 by using the equation $\tau = (\beta - \alpha)/60$, where β = O(1)−Cu(1)−N(3) (167.3°) and α = O(2)−Cu(1)−N(2) (146.4°) for the Cu(1) center and β = O(2)−Cu(2)−N(5) (159.1°) and α = O(1)−Cu(2)−N(4) (155.7°) for the Cu(2) center, respectively (for the perfect square-planar and trigonal-bipyramidal geometries, the values of τ are zero and unity, respectively).[31] The basal plane at the Cu(1) center comprises two pyridine nitrogen atoms, N(2) and N(3), and two phenolate oxygen atoms, O(1) and O(2), whereas the one for the Cu(2) center is occupied by one pyridine nitrogen atom, N(5), the tertiary amine nitrogen atom, N(4), and two phenolate oxygen atoms, O(1) and O(2). The copper ions, Cu(1) and Cu(2), are 0.257 and 0.357 Å above the planes and are axially coordinated to the tertiary amine nitrogen N(1) and a pyridine nitrogen, N(6), respectively.

It is interesting to note that the dihedral angles of the methylthio substituents and the phenol rings defined by C(8)−S(1)−C(6)−C(1) and C(31)−S(2)−C(29)−C(24) are 11° and 12° in the solid state, respectively, which are relatively small as compared to that in free $\mathbf{1}^-$ (60°) obtained by MO calculation (*vide ante*). This may indicate that, in the copper complex, the degree of the electronic interaction between the methylthio group and the phenolate moiety increases as compared to that in the free phenolate derivative, although the steric hindrance around the methylthio group in the solid state may also influence such steric geometry to some extent.

Copper complex **8** also has two nonequivalent five-coordinated metal ion centers coordinated by two pyridine nitrogen atoms, the tertiary amine nitrogen atom, and two phenolate oxygen atoms (Figure 8) as in the case of **7**. The copper−copper separation is 3.14 Å, and the geometries at the Cu(1) and Cu(2) centers are best described as distorted square-pyramidal with relative amounts of the trigonal−bipyramidal component, τ = 0.327 and 0.195, respectively [β = O(1)−Cu(1)−N(3) (167.5°) and α = O(2)−Cu(1)−N(2) (147.9°) for the Cu(1) center, and β = O(2)−Cu(2)−N(5) (164.3°) and α = O(1)−Cu(2)−N(4) (152.6°) for the Cu(2) center].[31] In this case as well, the basal plane at the Cu(1) center comprises two pyridine nitrogen atoms, N(2) and N(3), and two phenolate oxygen atoms, O(1) and O(2), whereas the equatorial plane for the Cu(2) center is occupied by one pyridine nitrogen atom, N(5), the tertiary amine nitrogen atom, N(4), and two phenolate oxygen atoms, O(1) and O(2). The copper ions are 0.264 and 0.335 Å above the basal planes and are axially coordinated to the tertiary amine nitrogen N(1) and a pyridine nitrogen, N(6), respectively. In both dimer complexes, **7** and **8**, the phenolate rings are located in the basal planes, which is consistent with the proposal that a copper complex of a tripodal ligand having a phenolate moiety with 6,6,6-membered chelate ring sequence tends to take the phenolate moiety as an equatorial ligand.[17f,g]

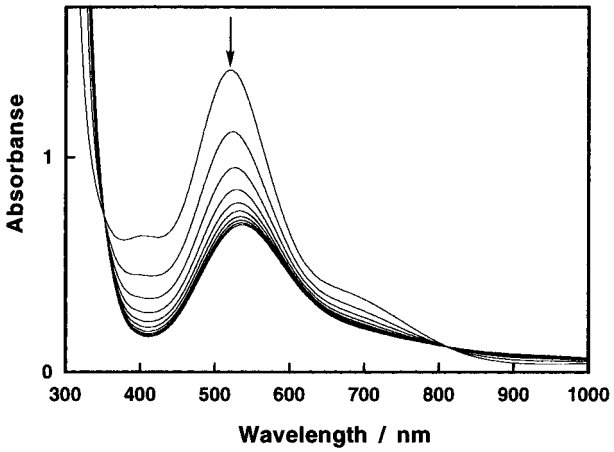

Figure 9. Spectral change observed upon addition of pyridine (0−0.3 M) into a CH_3CN solution containing **7** (2.5×10^{-4} M).

Dimer copper complexes **7** and **8** can be converted into the corresponding monomeric species by adding an exogenous ligand such as pyridine (py) into a CH_3CN solution of the dimer.[16] In the electrospray ionization mass spectrum (ESI-MS), a cationic species of the dimer $\{[Cu^{II}_2(\mathbf{3}^-)_2](PF_6)\}^+$ was detected at *m*/*z* 1057 as a major component in a CH_3CN solution of **7** (0.2 mM), while the monomeric species $[Cu^{II}(\mathbf{3}^-)]^+$ (M^+ = 455) became predominant when an excess amount of pyridine (5 vol %) was added into the solution.[32] A similar result was obtained in the case of **8**; $\{[Cu^{II}_2(\mathbf{4}^-)_2](PF_6)\}^+$ was detected at *m*/*z* 965 as a major component in a CH_3CN solution of **8** (0.2 mM), while $[Cu^{II}(\mathbf{4}^-)]^+$ was detected at *m*/*z* 409 as a major component when pyridine (10 vol %) was added into the solution.[32] In both cases, however, the peaks for the monomeric species involving added pyridine as a second ligand, $[Cu^{II}(\mathbf{L}^-)(py)]^+$, were very small, indicating that the binding of pyridine in those complexes is very weak.[33]

In Figure 9 is shown the spectral change observed upon addition of pyridine (0−0.30 M) into a CH_3CN solution of **7** (2.5×10^{-4} M). Dimer complex **7** has a low-energy phenolate-to-copper LMCT band at 520 nm (ϵ = 2800 M^{-1} cm^{-1} per Cu ion) together with a Cu(II) ligand field excitation (Cu(II) d−d

(31) Addison, A. W.; Rao, T. N. *J. Chem. Soc., Dalton Trans.* **1984**, 1349.

(32) Observed parent ion envelopes have isotope patterns consistent with the formulations indicated in the text.

(33) Pyridine may be dissociated from the ternary complex under the conditions of ESI-MS measurement.

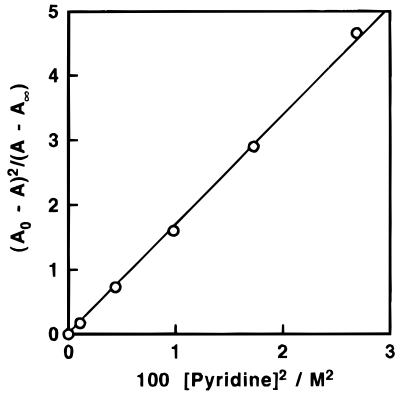

Figure 10. Plot of $(A - A_0)^2/(A - A_\infty)$ vs [pyridine]^2 for titration of **7** by pyridine in CH_3CN shown in Figure 9.

Table 5. Electronic Spectra of the Copper Complexes in CH_3CN

	λ_{max}/nm (ϵ/M^{-1} cm^{-1})	
compound	LMCT	ligand field
$[Cu^{II}_2(\mathbf{3}^-)_2](PF_6)_2$ (**7**)	520 (2800)	700 (675)
$[Cu^{II}(\mathbf{3}^-)(py)](PF_6)$ (**9**)	540 (1320)	752 (307)
$[Cu^{II}_2(\mathbf{4}^-)_2](PF_6)_2$ (**8**)	455 (3340)	665 (413)
$[Cu^{II}(\mathbf{4}^-)(py)](PF_6)$ (**10**)	508 (1260)	710 (254)

band) at 700 nm ($\epsilon = 675$ M^{-1} cm^{-1} per Cu ion).[34] The former absorption (LMCT) band is shifted to 540 nm ($\epsilon = 1320$ M^{-1} cm^{-1}) by the dissociation into the monomer complex $[Cu^{II}(\mathbf{3}^-)(py)](PF_6)$ (**9**), while the latter absorption around 700 nm shifted to 752 nm ($\epsilon = 307$ M^{-1} cm^{-1}).[34] From the spectral change, the association constant ($K_a = [\mathbf{9}]^2/[\mathbf{7}][py]^2$) of **7** with pyridine (py) was found to be 1.9×10^{-1} M^{-1} by using the equation $(A - A_0)^2/(A - A_\infty) = (1/4)K_a(\epsilon_7 - 2\epsilon_9)[py]^2$, where ϵ_7 and ϵ_9 are molar absorption coefficients of **7** and **9**, respectively. A plot of $(A - A_0)^2/(A - A_\infty)$ vs $[py]^2$ gave a linear line passing through the origin as illustrated in Figure 10 from which $(1/4)K_a(\epsilon_7 - 2\epsilon_9)$ was obtained as the slope. A similar spectral change was obtained with dimer complex **8,** and the K_a value was determined to be 1.5×10^{-3} M^{-1} in a similar manner. The larger association constant of **7** with external pyridine than that of **8** can be attributed to the steric hindrance of the methylthio group in the dimer. Dissociation of the dimer into the monomer by the coordination of pyridine will reduce the steric repulsion between the methylthio group and the pyridyl moiety of the ligand (see Figure 7). The LMCT and the Cu(II) d−d bands of the dimeric and monomeric species are summarized in Table 5. In both cases, addition of pyridine results in a shift of the spectral features to lower energy and a decrease in the intensity, accompanied by dissociation of the dimer into the monomer on coordination by pyridine.

In the electronic spectra, one can see a marked difference in the λ_{max} values between the model complexes having a methylthio substituent (**7** and **9**) and those without the substituent (**8** and **10**). The large red shifts of the LMCT and d−d bands of **7** and **9** as compared to those of **8** and **10** may be due to the delocalization of electron from the phenolate moiety into the sulfur atom of the SMe group of **7** and **9**. Such a large difference in λ_{max} is not seen in the free ligands **3H** and **4H** (see Table 1).

No ESR signal was detected for the dimer complexes **7** and **8** at low temperature, indicating that there is a strong antiferromagnetic coupling interaction in the μ-bridged Cu_2O_2 core. Addition of excess pyridine into the CH_3CN solution results in the appearance of an ESR signal [A and C in Figure 11],

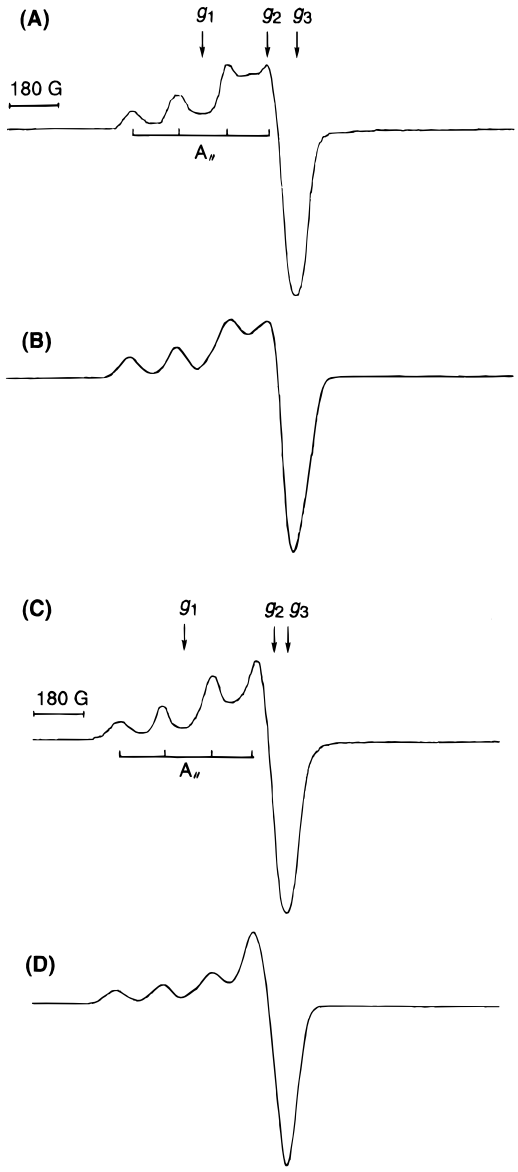

Figure 11. (A) ESR spectrum of $[Cu^{II}(\mathbf{3}^-)(py)](PF_6)$ (**9**) generated from $[Cu^{II}_2(\mathbf{3}^-)_2](PF_6)_2$ (**7**) (2.5×10^{-4} M) by adding pyridine (1.8×10^{-2} M) in CH_3CN; 77 K, microwave frequency 9.03 GHz, modulation frequency 100 kHz, modulation amplitude 8 G, microwave power 8 mW. (B) Computer simulation spectrum with the parameters $g_1 = 2.250$, $g_2 = 2.085$, $g_3 = 2.012$, and $A_{\parallel} = 180$ G. (C) ESR spectrum of $[Cu^{II}(\mathbf{4}^-)(py)](PF_6)$ (**10**) generated from $[Cu^{II}_2(\mathbf{4}^-)_2](PF_6)_2$ (**8**) (2.5×10^{-4} M) by adding pyridine (0.5 M) in CH_3CN; 77 K, microwave frequency 9.00 GHz; modulation frequency 100 kHz; modulation amplitude 8 G; microwave power 8 mW. (D) Computer simulation spectrum with the parameters $g_1 = 2.257$, $g_2 = 2.052$, $g_3 = 2.037$, and $A_{\parallel} = 180$ G.

consistent with the former results of ESI-MS and UV−vis indicating monomer complex formation. Computer simulation of the spectra [B and D in Figure 11] provided us with the ESR parameters of $g_1 = 2.250$, $g_2 = 2.085$, $g_3 = 2.012$, and $A_{\parallel} = 180$ G for **9** and $g_1 = 2.257$, $g_2 = 2.042$, $g_3 = 2.020$, and $A_{\parallel} = 175$ G for **10**. These values are very close to those of galactose oxidase[35] and of the reported model copper(II) complexes having distorted square-pyramidal structures.[16,17d] The ligand field absorptions of **9** and **10** are also consistent with a distorted square-pyramidal structure of the monomer Cu(II) complex.[17f]

Figure 12 shows the cyclic voltammograms of **9** and **10** generated from **7** and **8** by adding excess amounts of pyridine

(34) Since the Cu(II) d−d band is not so clear, the λ_{max} was estimated by analyzing the spectrum using Gaussian functions.

(35) Winkler, M. E.; Bereman, R. D. *J. Am. Chem. Soc.* **1980**, *102*, 6244.

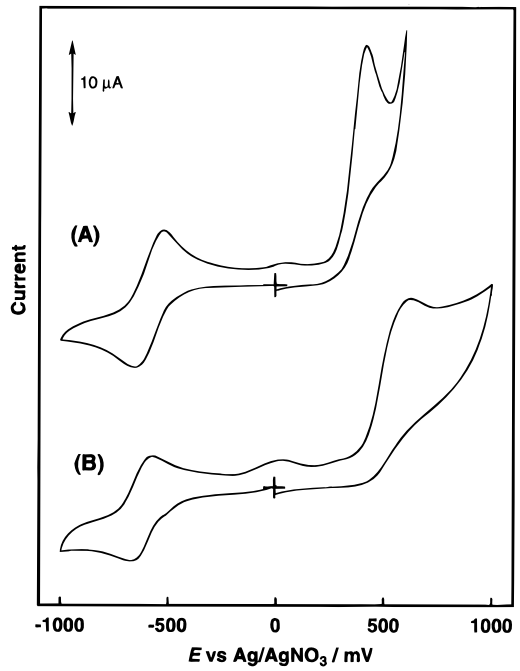

Figure 12. Cyclic voltammograms of (A) $[Cu^{II}(\mathbf{3}^-)(py)](PF_6)$ (**9**) generated from $[Cu^{II}_2(\mathbf{3}^-)_2](PF_6)_2$ (**7**) (1.5×10^{-3} M) by adding pyridine (0.5 M) in CH_3CN containing 0.1 M NBu_4ClO_4 and (B) $[Cu^{II}(\mathbf{4}^-)(py)](PF_6)$ (**10**) generated from $[Cu^{II}_2(\mathbf{4}^-)_2](PF_6)_2$ (**8**) (1.5×10^{-3} M) by adding pyridine (0.5 M) in CH_3CN containing 0.1 M NBu_4ClO_4; working electrode Pt, counter electrode Pt wire, reference electrode Ag/0.01 M $AgNO_3$, scan rate 100 mV s^{-1}.

in CH_3CN containing 0.1 M NBu_4ClO_4.[36] Monomer complex **9** exhibits a reversible redox wave for the Cu(II)/Cu(I) couple at −591 mV vs $Ag/AgNO_3$ (−301 mV vs SCE) and an irreversible anodic peak for the oxidation of the ligand phenolate moiety at 415 mV vs $Ag/AgNO_3$ (705 mV vs SCE), while **10** shows a reversible peak for the Cu(II)/Cu(I) couple at −622 mV vs $Ag/AgNO_3$ (−332 mV vs SCE) and an irreversible anodic peak for the oxidation of the ligand phenolate moiety at 623 mV vs $Ag/AgNO_3$ (913 mV vs SCE). In order to determine the redox potential of the ligand moiety in the monomer copper complexes, we employed the fast cyclic voltammetric method using an Au microelectrode. As shown in Figure 13, **9** gave a reversible wave at 370 mV vs $Ag/AgNO_3$ (660 mV vs SCE) when the measurement was carried out at a scan rate of 100 V s^{-1}.[36] On the other hand, however, no reversible wave for complex **10** has been observed even at a faster scan rate (300 V s^{-1}). This result clearly indicates that the stability of the radical species of **9** is much higher than that of **10**, reflecting the radical stabilizing effect of the methylthio group as mentioned above. As in the case of the free ligand (Table 1), the redox potential of the phenolate moiety of **9** is lower than that of **10** by about 200 mV. This result can also be explained by taking into account both the electron-donating effect and electron-sharing conjugation (radical stabilization) by the methylthio group mentioned above. Delocalization of the negative charge of the phenolate moiety into the methylthio substituent can also be realized by the positive shift of the redox potential at the copper site (−332 to −301 mV vs SCE).

In our model system, we observed about a 200 mV negative shift of the oxidation peak of the ligand by introducing the methylthio group into the phenol ring. In the enzymatic system, however, a more than 500 mV negative shift of the redox potential of the cofactor of galactose oxidase (GOase) has been reported.[3] Such a difference between our model system and the enzymatic system may indicate that there is another factor which lowers the redox potential of the cofactor. The X-ray structure of GOase clearly indicates that there is a $\pi-\pi$ stacking interaction between the cofactor and Trp 290 in the enzyme active site.[6] This may be an additional important factor to stabilize the phenoxyl radical species of the cofactor, lowering its redox potential.

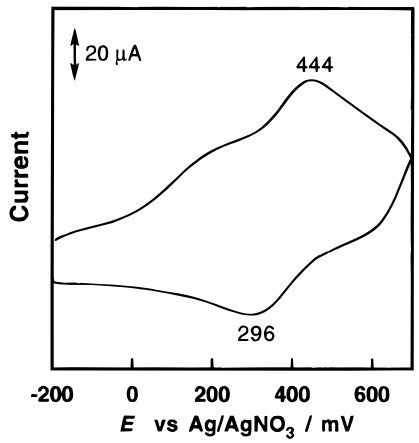

Figure 13. Fast cyclic voltammogram of the ligand moiety of $[Cu^{II}(\mathbf{3}^-)(py)](PF_6)$ (**9**) generated from $[Cu^{II}_2(\mathbf{3}^-)_2](PF_6)_2$ (**7**) (1.5×10^{-3} M) by adding pyridine (0.5 M) in CH_3CN containing 0.1 M NBu_4ClO_4; working electrode Au microelectrode, counter electrode Pt wire, reference electrode Ag/0.01 M $AgNO_3$, scan rate 100 V s^{-1}.

Concluding Remarks

The present study is aimed mainly at revealing the electronic effect of the thioether group in the novel organic cofactor of galactose oxidase and glyoxal oxidase. The electron-donating nature of the thioether group in both the neutral and anionic forms of the cofactor models is implicated by the observed upfield shifts of the aromatic protons of the model compounds having the methylthio substituent as compared to those of the compounds without the substituent. On the other hand, the lower pK_a values of **1H** and **2H** as compared to that of **5H** indicate that the methylthio group also has a $2p\pi-3d\pi$ electron conjugative effect, stabilizing the negative charge on the phenolate oxygen. Furthermore, the electron-sharing conjugative effect of the sulfide group in the radical state has been clearly demonstrated by the ESR studies and theoretical calculations. The relatively large negative shift of the E°_{ox} values of the model compounds having the methylthio substituent as compared to that of the corresponding phenol derivatives without the substituent has been attributed to both the electron-donating nature and the radical stabilizing effect (electron-sharing conjugative effect) of the sulfide group. Electrochemical analysis of the copper complexes also reveals that the methylthio substituent in the copper complex shows electronic effects similar to those in the free ligand stabilizing the phenoxyl radical state of the cofactor moiety in the Cu(II) complex.

In order to understand the mechanism of the enzymatic redox reaction, however, we need to further address the following points. In the enzymatic redox reaction, it has also been proposed that the axially coordinated tyrosine (Tyr 495, see Scheme 1) plays important roles in controlling the redox potential of the copper center and to abstract a proton as a base from the substrate OH group, enhancing the electron donor ability of the substrate.[9] How can we build up such functions

(36) The small extra peaks that appear in the CVs for monomer complexes **9** and **10** (at ca. 50 mV in Figure 12 and ca. 200 mV in Figure 13) have not been assigned yet. However, those peaks could be attributed to a compound adsorbed on the electrode surface, since the small peaks were getting bigger during repeated scans of the electrochemical measurement.

of a weakly coordinated phenol in model systems? We have to also reveal how important the radical stabilizing effect by the $\pi-\pi$ stacking interaction between the cofactor and Trp 290 is. With regard to the alcohol-oxidation reaction at a Cu(II)-phenoxyl radical site, Tolman et al. and Stack et al. recently reported the first functional models of galactose oxidase to provide valuable insight into the alcohol-oxidation mechanism.[37] On the other hand, very little is known about the reoxidation process of the Cu(I)-phenolate state to the Cu(II)-phenoxyl radical state by molecular oxygen. Judging from the redox potential of the copper ion and the cofactor moiety of our system, oxidation of Cu(I) to Cu(II) is very easy, but oxidation of the phenolate to the phenoxyl radical may not be so easy via a simple electron transfer mechanism. In fact, the Cu(II)-phenolate state is most stable in all the model complexes so far reported as well as in the enzymatic system. Thus, the two-electron oxidation of the Cu(I)-phenolate state to the Cu(II)-phenoxyl radical state by molecular oxygen may proceed in a coordination sphere of the copper site probably through a superoxocopper(II) species.

(37) (a) Halfen, J. A.; Young, V. G., Jr.; Tolman, W. B. *Angew. Chem.* **1996**, *108*, 1832. (b) Wang, Y.; Stack, T. D. P. *J. Am. Chem. Soc.* **1996**, *118*, 13097.

Acknowledgment. The present study was financially supported in part by a Grant-in-Aid for Scientific Research on Priority Area (08249223) and a Grant-in-Aid for General Scientific Research (08458177) from the Ministry of Education, Science, Sports, and Culture of Japan and also by Takeda Science Foundation. We also thank Professor Yasushi Kai and his co-workers, particularly, Dr. Nobuko Kanehisa and Mr. Hiroshi Hashimoto of Osaka University, for their assistance in the X-ray measurements.

Supporting Information Available: The SOMO and LUMO of **1**• calculated by the PM3 method. Complete drawings and full details of the X-ray structure determination, including tables of fractional atomic coordinates and interatomic bond distances and angles for **7** and **8** (42 pages). Ordering information is given on any current masthead page.

IC961144A